

Effect of Surface Chemical Bonding States on Lithium Intercalation Properties of Surface-Modified Lithium Cobalt Oxide

Jun-Ichi Hata,^[a] Masaaki Hirayama,^{*[a]} Kota Suzuki,^[a] Nicolas Dupré,^[b] Dominique Guyomard,^[b] and Ryoji Kanno^[c]

Understanding interfacial reactions between surface-modified lithium intercalation cathodes and organic electrolytes facilitates the design of highly functional cathodes for lithium-ion batteries. Here, the chemical bonding state between a LiCoO₂ cathode and a ZrO_{2-x} surface layer is controlled by pulsed arc plasma deposition using different ion energies. The lithium intercalation properties and interfacial structure changes are subsequently analyzed. The Zr–O–Co-modified surface formed

by interaction between ZrO_{2-x} and LiCoO₂ provides superior cycle stability under high-voltage operation (2.8–4.5 V). X-ray photoemission spectroscopy clarifies that the Zr–O–Co surface forms highly adhesive ZrO_xF_y as a cathode electrolyte interphase (CEI). The chemical bonding state at the ZrO_{2-x}/LiCoO₂ interface affects the reactivity of ZrO_{2-x} with electrolyte species as well as the architecture of the CEI, which may determine the cell performances of lithium intercalation cathodes.

1. Introduction

With the ever-increasing demand for lithium-ion batteries with high energy density, it is crucial to stabilize charge-discharge reactions of lithium-intercalation electrodes under high-voltage operation (i.e., above 4.5 V). Surface modification with metal oxides such as Al₂O₃,^[1] MgO,^[2] ZrO₂,^[3] and Li₂ZrO₃,^[4] has been reported to be an efficient method of improving cycle performance and rate capability of intercalation electrodes. Several roles of the modification layer have been proposed: (i) The modification layer suppresses direct contact of the electrode with the electrolyte, which prevents undesired reactions at the interface such as excessive decomposition of electrolyte species and dissolution of transition metals from the electrode.^[5] (ii) The modification layer could react with electrolyte species, resulting in the formation of an interfacial layer that includes lithium-ion conductive phases. Such an interfacial layer would help to stabilize the electrode/electrolyte interface and enhance

the rate of lithium-ion transfer.^[6] (iii) The crystal structure at the electrode surface could be stabilized by doping of metal atoms from the coating layer and by the pillar effect.^[2,7] (iv) The modification layer located at grain boundaries in polycrystalline electrodes could prevent particle cracking during charge-discharge cycling.^[8] However, there has been no unified understanding that allows controlled interphase formation and optimized electrode properties. One of the main reoccurring issues concerns the reproducibility of coating layers' properties. The coating effects change significantly in response to synthetic methods and conditions, even for the same combination of electrode and coating material.^[9] Generally, the interaction between the coating material and the intercalation electrode leads to redistribution of electrons and ions, which can alter the properties of both at the interface. Considering that the thickness of the coating layer is ~10 nm in most cases, the ionic conductivity of the coating material and reactivity with the electrolyte species should be affected by the chemical bonding at the interface with the active material. The bonding states at the interface should change under synthesis methods and their process conditions. However, the modified-electrode/electrolyte interface is designed from expectations based on the structure and properties of bulk materials. It is therefore important to evaluate the bonding states between the electrodes and coating material, and to clarify how this affects the interfacial reactions that occur during charging and discharging.

Pulsed arc plasma deposition (APD) is a physical vapor deposition (PVD) technique that is distinctive for its high activity of evaporated species, derived from high ionization rates and ion energies.^[10] When the plasma ions collide with the substrate or the grown film, substantial ion energy is supplied due to the inherent kinetic energy; ionization energy is released during ion-electron recombination; and cohesive energy is released by chemical bond formation between depositing and substrate species. The substantial amount of ion energy

[a] J.-I. Hata, Prof. M. Hirayama, Dr. K. Suzuki
Department of Chemical Science and Engineering
School of Materials and Chemical Technology
Tokyo Institute of Technology
4259 Nagatsuta, Midori-ku, Yokohama, 226-8502, Japan
E-mail: hirayama@echem.titech.ac.jp

[b] Dr. N. Dupré, Prof. D. Guyomard
Institut des Matériaux Jean Rouxel (IMN)
Université de Nantes, CNRS UMR 6502
Institut des Matériaux Jean Rouxel
2 rue de la Houssinière, BP32229, Nantes Cedex 3 44322, France

[c] Prof. R. Kanno
All-Solid-State Battery Unit
Institute of Innovative Research
Tokyo Institute of Technology
4259 Nagatsuta, Midori-ku, Yokohama 226-8503, Japan

 Supporting information for this article is available on the WWW under <https://doi.org/10.1002/batt.201800122>

 An invited contribution to a Special Issue on SEI and Interphases at Electrodes

enhances the mobility of deposited atoms in the surface region of the substrate/film. Furthermore, the ion energy of the plasma ions is controllable, as the collision frequency can be modulated by altering the gases that fill the chamber; the frequency is determined by the gas pressure as well as the voltage and capacitance of the arc discharge. These features enable modification of the chemical bonding states at the interface between the depositing and substrate species.^[11] One distinctive application of this approach is surface coating.^[10,12] The coating layers fabricated by APD with a moderately high ion energy are highly uniform and adhesive, even when fabricated at room temperature,^[13] compared to those synthesized by other PVD techniques. Thus, the APD technique has been applied to synthesize TiN and ZrN as well as ZrO₂ films as coatings.^[14] However, there have been no reports of applying APD with surface coatings to lithium battery electrode materials.

In this study, we fabricate a thin-film model electrode of LiCoO₂ and modify the LiCoO₂ surface by depositing ZrO_{2-x} using the APD method under different oxygen pressures. The ion energy of the zirconium plasma is changed by modulating the collision frequency with oxygen, which leads to different bonding states between the LiCoO₂ and the ZrO_{2-x} coating layer. The structure and surface morphology are characterized by X-ray diffraction (XRD), Raman spectroscopy, atomic force microscopy (AFM), field emission scanning electron spectroscopy (FE-SEM), and X-ray photoemission spectroscopy (XPS). Electrochemical charge-discharge measurements are conducted in the voltage range of 2.8–4.5 V to investigate the effect of ZrO_{2-x}-modified bonding state on cyclic stability under high-voltage operation. The XPS analyses detect the species in the interfacial layer formed at the LiCoO₂ surfaces during electrochemical cycling. The relationship among the chemical bonding states formed at the initial surface, cathode electrolyte interphase (CEI) layer formation, and cycle retention during high-voltage charging-discharging are discussed.

2. Results and Discussion

2.1. Structural Characterization of LiCoO₂ Films

Figure 1 shows the XRD pattern, Raman spectrum, and surface SEM image of the unmodified LiCoO₂ film synthesized on a Au substrate by RF magnetron sputtering. All diffraction peaks of the films are attributed to LiCoO₂ with a layered rocksalt structure with the space group *R*-3 *m* (Figure 1a). The lattice parameters are calculated to be $a=2.8175(2)$ Å and $c=14.076(4)$ Å, which are consistent with those reported previously.^[3,15] LiCoO₂ films often contain Co₃O₄ and/or cubic LiCoO₂ as low-temperature phases.^[16] However, these phases are difficult to detect using XRD because their diffraction peaks appear at similar angles to those of layered rocksalt LiCoO₂.^[17] In the Raman spectrum, two sharp peaks are observed at 492 cm⁻¹ and 601 cm⁻¹ (Figure 1b). These peaks are attributed to the E_g vibration (O–Co–O bending) and A_{1g} vibration (O–Co–O stretching) modes of the layered rocksalt LiCoO₂,

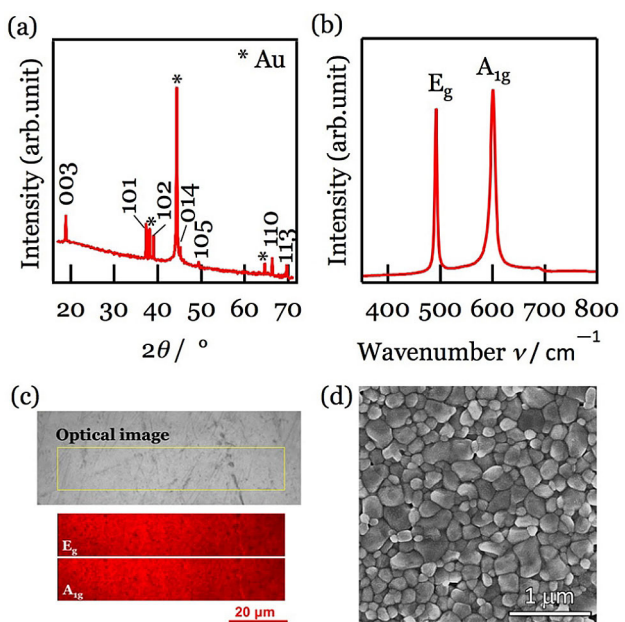


Figure 1. (a) XRD pattern, (b, c) Raman spectrum and mapping image for E_g and A_{1g} vibration modes, and (d) surface SEM image of the LiCoO₂ film synthesized on an Au substrate by RF magnetron sputtering.

respectively.^[18] No Raman peaks derived from Co₃O₄ (a clear peak around 690 cm⁻¹) or cubic LiCoO₂ (doublet peaks around 600 cm⁻¹) can be observed in the spectrum. Furthermore, the mapping image of the E_g and A_{1g} vibration modes reveals the uniform formation of layered rocksalt LiCoO₂ on a microscopic scale. The surface SEM image shows densely gathered LiCoO₂ domains with a size of a few hundred nanometers (Figure 1d). The XRD, Raman spectroscopy, and SEM results confirm that the film was composed of single-phase domains of layer rocksalt LiCoO₂, which is suitable for analyzing the effects of surface modification on interfacial phenomena with organic electrolytes.

2.2. Chemical Bonding States at ZrO_{2-x} Modified Surfaces

Prior to surface modification of the LiCoO₂ film with zirconium oxide, the ZrO_{2-x} modification was conducted on Al₂O₃ (0001) single-crystal surfaces to investigate the effect of the ion energy of zirconium plasma on the bonding states between the zirconium oxide and substrate species. Investigation of the structural changes at the ZrO_{2-x}/Al₂O₃ interface by XPS. Figure 2 shows the Al 2p, Zr 3d, and O 1s XP spectra of the unmodified and ZrO_{2-x}-modified Al₂O₃ substrate. The ZrO_{2-x} deposition was performed under different oxygen pressures of 30 Pa, 1 Pa, and 3×10^{-4} Pa in a vacuum chamber of the APD system. The thickness of the ZrO_{2-x} modification layer could be estimated to be 0.4 nm from the deposition rate (0.1 nm pulse⁻¹), which is thin enough to facilitate the Al 2p and O 1s peaks of the unmodified Al₂O₃ (0001) substrate can be observed at 74.0 eV and 530.8 eV, respectively; these values are consistent with those reported previously.^[19] The peak at 532 eV in the O 1s spectra is attributed

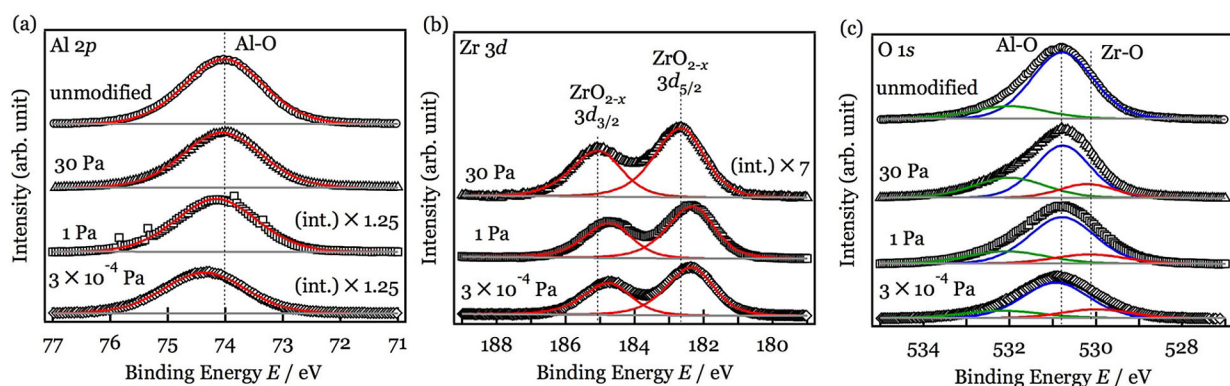


Figure 2. XP spectra of (a) Al 2p, (b) Zr 3d, and (c) O 1s of unmodified and 0.4-nm-thick ZrO_{2-x} modified Al_2O_3 (0001) substrates. The oxygen pressures used during ZrO_{2-x} deposition were set to 30 Pa, 1 Pa, and 3×10^{-4} Pa.

to an adventitious carbon layer on the substrate.^[20] The $\text{ZrO}_{2-x}/\text{Al}_2\text{O}_3$ interface synthesized under an oxygen pressure of 30 Pa shows no significant changes in the positions of the Al 2p and O 1s peaks. The Zr 3d_{5/2} and Zr 3d_{3/2} peaks are observed at 182.7 eV and 185.1 eV, which are attributed to oxygen-deficient ZrO_{2-x} .^[21] Chemical bonding could not be observed between Al_2O_3 and ZrO_{2-x} . This could be associated with the low ion energy of Zr ions remaining after their frequent collisions with oxygen molecules during their flight in the chamber, as described in the supplemental information (S1). In contrast, the $\text{ZrO}_{2-x}/\text{Al}_2\text{O}_3$ interfaces synthesized under oxygen pressures of 1 Pa and 3×10^{-4} Pa show a slight shift of the Al 2p peak to higher binding energy (B.E.) values of 74.2 eV and 74.4 eV, respectively. Furthermore, the Zr 3d_{5/2} and Zr 3d_{3/2} peaks shift to lower B.E. values of 182.4 eV and 184.8 eV. These results indicate that the valence states change from Al^{3+} to $\text{Al}^{(3+\alpha)+}$ and from Zr^{4+} to $\text{Zr}^{(4-\alpha)+}$. The highly energetic Zr ions affect the bonding states of the Al ions. From above, the formation of Al–O–Zr chemical bonding at the $\text{ZrO}_{2-x}/\text{Al}_2\text{O}_3$ interface is suggested. The O 1s spectra for all

modified samples show a small peak at 530.1 eV in addition to the peaks observed in the unmodified sample, which could be attributed to Zr–O bonding in ZrO_{2-x} .^[22] It is confirmed that high-energy evaporated species generated by the APD process could lead to chemical bonding at the surface.

Figure 3 depicts the Co 2p, O 1s, and Zr 3d XP spectra of the unmodified and 0.4-nm-thick ZrO_{2-x} -modified LiCoO_2 films. The unmodified LiCoO_2 surface shows the Co 2p peak at 780.1 eV with a shoulder region at high binding energies (Figure 3a). The peak position is attributable to Co^{3+} in the LiCoO_2 lattice, which is supported from the satellite peaks observed at around 790 eV.^[23] The shoulder region can be identified as Co^{4+} in Li-deficient $\text{Li}_{1-x}\text{Co}^{\text{III/IV}}\text{O}_2$.^[24] From the spectrum fitting, the integrated-intensity ratio of the Co^{4+} to Co^{3+} peaks ($I_{\text{Co}4+}/I_{\text{Co}3+}$) is 1.0 for the unmodified LiCoO_2 film. The O 1s peaks are observed at 529.5 eV and 531.5 eV (Figure 3b), which corresponds to lattice oxygen in LiCoO_2 and Li_2CO_3 , respectively.^[6b,25] These results indicate that the typical chemical reaction of LiCoO_2 with CO_2 in ambient air occurred, resulting in the formation of $\text{Li}_{1-x}\text{Co}^{\text{III/IV}}\text{O}_2$

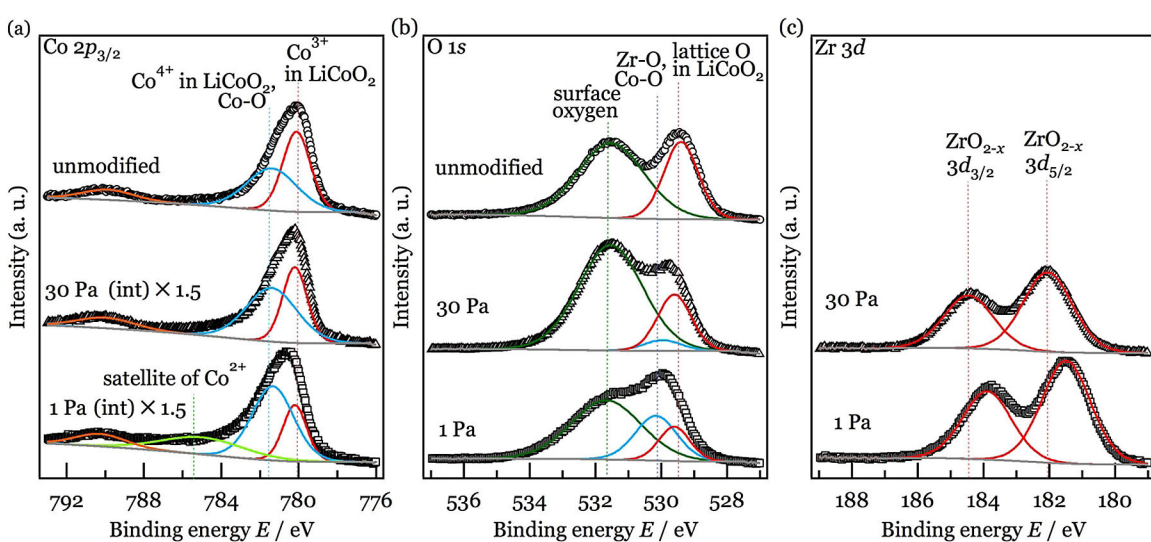


Figure 3. (a) Co 2p, (b) O 1s and (c) Zr 3d XP spectra of unmodified and 0.4-nm-thick ZrO_{2-x} modified LiCoO_2 film under different oxygen pressures of 30 Pa and 1 Pa.

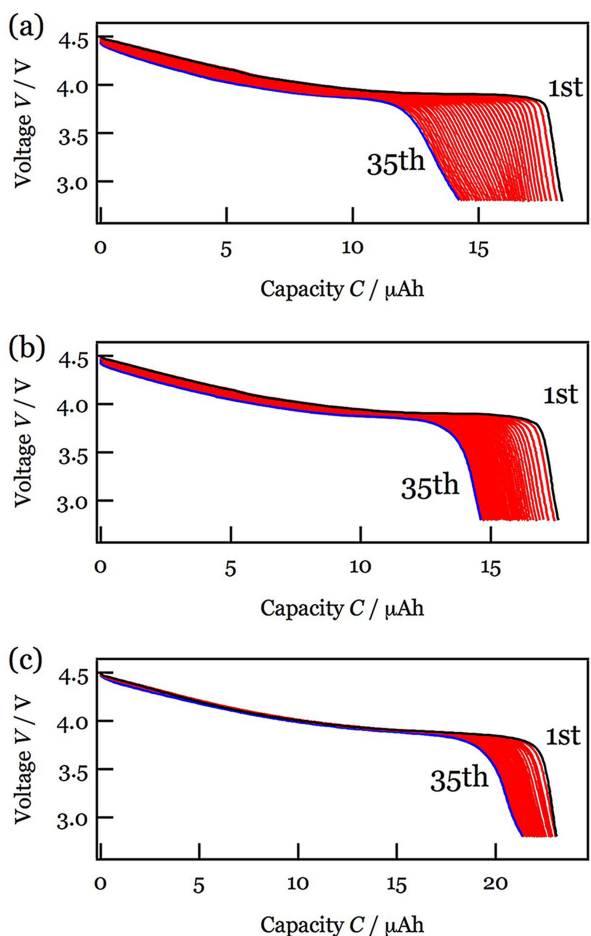


Figure 4. Discharge curves of (a) the unmodified LiCoO₂ film and (b, c) ZrO_{2-x}-modified LiCoO₂ films. ZrO_{2-x} films were modified under oxygen pressures of (b) 30 Pa and (c) 1 Pa. Expected thicknesses of the films were 500 nm (a,b) and 570 nm (c).

and Li₂CO₃ at the surface. For the ZrO_{2-x}/LiCoO₂ interface synthesized under an oxygen pressure of 30 Pa, the $I_{\text{Co}^{4+}}/I_{\text{Co}^{3+}}$ value increases slightly to 1.4 with a small shift of the Co 2p peak to higher binding energies. By the ZrO_{2-x} modification, the LiCoO₂ surface may change to three possible phases: lithium deficient Li_{1-x}Co^{III/IV}O₂, Li_{1-x}Co^{III}_{1-2x}Zr^{IV}_xO₂ solid-solution, and LiCo^{II}_xCo^{III}_{1-2x}Zr^{IV}_xO₂ solid-solution. The further formation of Li_{1-x}Co^{III/IV}O₂ is consistent with the increase in the Co⁴⁺ component and the high intensity of the Li₂CO₃ peak in the O 1s spectrum compared to that of the unmodified Li_{1-x}Co^{III/IV}O₂ (Figure 3b). When Li_{1-x}Co^{III}_{1-2x}Zr^{IV}_xO₂ and LiCo^{II}_xCo^{III}_{1-2x}Zr^{IV}_xO₂ solid-solutions are formed, the Co⁴⁺ component should not increase. Hence, the ZrO_{2-x} modification causes no solid-solutions, which is consistent with experimental and calculation studies that have reported no solid-solution phase formation at the ZrO_{2-x}/LiCoO₂ interface.^[26] As no other chemical bonding states are observed, it can be concluded that the ZrO_{2-x} modification under an oxygen pressure of 30 Pa causes further formation of Li_{1-x}Co^{III/IV}O₂ at the surface region. At the LiCoO₂ surface modified by ZrO_{2-x} under 1 Pa, the $I_{\text{Co}^{4+}}/I_{\text{Co}^{3+}}$ value significantly increased to 2.3 at the LiCoO₂ surface modified by ZrO_{2-x} under 1 Pa, and a Co²⁺ satellite peak was observed at around 785.5 eV.^[27] A clear peak

can be observed at 530.1 eV in the O 1s peak of the LiCoO₂ surface modified by ZrO_{2-x} under 1 Pa. Considering that the Zr 3d peaks have similar relative intensities to those observed for the film modified under 30 Pa (Figure 3c), the significant increase in intensity of the 530.1 eV peak indicates the formation of oxides other than ZrO_{2-x} and LiCo^{II}_xCo^{III}_{1-2x}Zr^{IV}_xO₂. Thus, the peak observed at 530 eV can be attributed to Co–O bonding in simple oxides such as CoO and Co₃O₄.^[22,24b] Furthermore, the Zr 3d_{5/2} and 3d_{3/2} peaks are observed at 181.5 and 183.9 eV, which are shifted to lower B.E. values than those under 30 Pa (182.0 and 184.4 eV, respectively). The Zr 3d_{5/2} peak of Zr⁴⁺ in ZrO₂ locates at 182.9 ± 0.1 eV and 185.2 ± 0.1 eV,^[21] therefore, the modification layer seems to exhibit oxygen deficiency to some extent or chemical bonding with an element other than Zr. Although deposition of Zr species under an oxygen pressure of 30 Pa could form weak Zr–O–Zr bonds with the LiCoO₂ surface, the deposition of highly energetic Zr species under an oxygen pressure of 1 Pa changes the Co–O and Zr–O bonding states and probably forms Zr–O–Co bonds at the LiCoO₂ surface. No significant changes in the crystal structure or morphology are observed in the XRD pattern or FE-SEM image of the LiCoO₂ film modified under an oxygen pressure of 1 Pa, which confirms that the surface modification did not affect the bulk structure of the LiCoO₂ film (See the supplemental information (S2)). These results show clearly that the interaction between LiCoO₂ and ZrO_{2-x} changes with the ion energy of the Zr species controlled by oxygen pressure in the chamber.

2.3. Lithium (De)intercalation Properties of ZrO_{2-x} Modified LiCoO₂

Figure 4 shows discharge curves of the unmodified and 0.4-nm-thick ZrO_{2-x}-modified LiCoO₂ electrodes. The discharge curves for all films clearly exhibit a plateau region at around 3.9 V and a sloped region in the higher-voltage region. The plateau region corresponds to the two-phase reaction between rhombohedral Li_{0.9}CoO₂ and Li_{0.78}CoO₂ phases, and the sloped region corresponds to lithium (de)intercalation of rhombohedral Li_{1-x}CoO₂ (0.22 ≤ x ≤ 0.45, 0.54 ≤ x ≤ 0.78) and monoclinic Li_{1-x}CoO₂ (0.45 ≤ x ≤ 0.54) phases.^[28] These results reveal the intercalation activity of the unmodified and ZrO_{2-x}-modified LiCoO₂ films. In the following section, we discuss the cycle retention of their electrochemical properties. Table 1 summarizes the discharge capacities and the average discharge voltages of the unmodified and ZrO_{2-x}-modified LiCoO₂ electro-

Table 1. Discharge capacity retention and average discharge voltage of unmodified LiCoO₂ and 0.4-nm-thick ZrO_{2-x}-modified LiCoO₂ films under oxygen pressures of 30 Pa and 1 Pa. The discharge capacity retention was normalized by the first discharge capacity in each sample.

	Discharge capacity retention 1 st	Average discharge voltage (V)				
		15 th	35 th	1 st	15 th	35 th
(a) unmodified	1 (normalized)	0.89	0.78	3.82	3.78	3.71
(b) 30 Pa	1	0.90	0.83	3.85	3.80	3.75
(c) 1 Pa	1	0.98	0.93	3.86	3.84	3.81

des. The discharge capacity of the unmodified LiCoO_2 electrode dramatically decreases with the number of cycles, and the retention at the 35th cycle is 0.78 when normalized by that in the 1st cycle. Simultaneously, the average discharge voltage dropped from 3.82 V at the first cycle to 3.71 V at the 35th cycle. Rapid degradation of battery performance with LiCoO_2 electrodes at voltages above 4.4 V has been reported by many research groups.^[29] The proposed deterioration mechanisms in high voltage operation have been interpreted as follows: 1) irreversible structural change of LiCoO_2 such as deterioration in the stacking of O–Co–O layers and formation of spinel phase,^[28b,30] and 2) Co dissolution and deposition of electrolyte decomposition compounds.^[31] The ZrO_{2-x} -modified LiCoO_2 electrode (30 Pa) exhibits a discharge capacity retention of 0.83 and an average discharge voltage of 3.75 V at the 35th cycle. Minor improvement of cycle stability is achieved by the surface zirconium species, which forms a weak bond with LiCoO_2 . In contrast, the ZrO_{2-x} -modified LiCoO_2 electrode (1 Pa) delivers a superior discharge capacity retention of 0.93 compared to the unmodified film and the ZrO_{2-x} -modified electrode (30 Pa). The average discharge voltage is 3.86 V in the 1st cycle and remains relatively stable at 3.81 V by the 35th cycle. It should be noted that the ZrO_{2-x} -modified electrode (1 Pa) shows no significant change in the capacity and average discharge voltage in the high-voltage regions (>4.0 V). Thus, we can speculate that no severe deterioration of the LiCoO_2 active material occurs in the ZrO_{2-x} -modified electrode (1 Pa).^[29b] The capacity decrease could be associated with another factor such as physical peeling of LiCoO_2 from the Au substrate by volumetric changes during charging and discharging.

2.4. Cathode Electrolyte Interphases at ZrO_{2-x} Modified LiCoO_2

To investigate changes to the surface structure during the initial stage of charge–discharge cycling, *ex situ* XPS was performed after the 10th discharging. Figure 5 presents the $\text{Co} 2p_{3/2}$, $\text{O} 1s$, and $\text{Zr} 3d$ XP spectra of the unmodified and 0.4 nm ZrO_{2-x} -modified LiCoO_2 films after charge–discharge cycling. The $\text{Co} 2p_{3/2}$ spectra of the cycled films consist of the components Co^{3+} and Co^{4+} in LiCoO_2 and cobalt oxides, along with the related satellite peaks, which are independent of the initial surface states formed by the ZrO_{2-x} modification, regardless of oxygen pressure (Figure 5a). Although the relative intensities of these peaks differ slightly between the unmodified and modified samples, the lithium (de)intercalation through the electrochemical interface leads to a similar Co chemical bonding state at the LiCoO_2 surface. In contrast to the $\text{Co} 2p$ spectra, the $\text{O} 1s$ spectra were significantly changed from those of the initial surface states (Figure 5b). All spectra were analyzed with six previously reported oxygen components: O in the LiCoO_2 lattice (529.4 eV), O in metal oxides such as Zr–O and Co–O (530.2 eV), inorganic compounds in the CEI such as LiOH and ZrO_xF_y (531.0 eV),^[6b,32] C=O bonds in Li_2CO_3 and Li alkyl carbonates (532.0 eV),^[33] C–O bonding in Li alkyl carbonates (533.5 eV),^[33b] and O in $\text{Li}_x\text{PF}_y\text{O}_z$ (534.5 eV).^[34] At the unmodified LiCoO_2 surface, the relative peak intensities of the CEI components (Li_2CO_3 , LiOH , and Li alkyl carbonates) are smaller than those of O^{2-} in the LiCoO_2 lattice. The LiCoO_2 surface modified by ZrO_{2-x} under 30 Pa shows an $\text{O} 1s$ spectrum similar to that of the unmodified surface. This suggests that no significant change occurs in the organic components of CEI, due to the small amount of the ZrO_{2-x} modification conducted with low ion energy Zr species. In contrast, the relative peak intensities of O^{2-} in the LiCoO_2 lattice strongly decreased after charge–discharge cycling in the case of the LiCoO_2 surface modified by ZrO_{2-x} under 1 Pa. These results highlight more rapid growth of

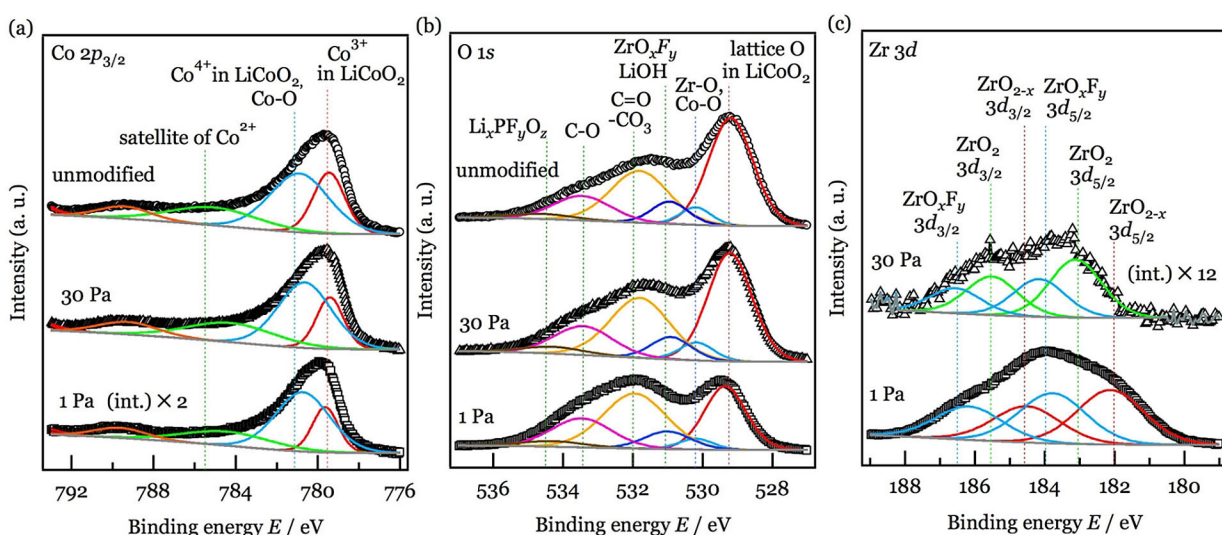


Figure 5. (a) $\text{Co} 2p$, (b) $\text{O} 1s$, and (c) $\text{Zr} 3d$ XP spectra of the unmodified LiCoO_2 and the ZrO_{2-x} -modified LiCoO_2 films after being discharged to 2.8 V at the 10th cycle. The ZrO_{2-x} modification was performed under different oxygen pressures of 30 Pa and 1 Pa.

the CEI layer at the LiCoO_2 surface after this modification with high energy Zr species. This is consistent with previous work, i.e., a substantial CEI layer is observed to grow in metal-oxide-modified LiCoO_2 but not on the unmodified LiCoO_2 surface.^[33b] Furthermore, the chemical bonding state of Zr atoms after the 10th discharging varied with the initial bonding state between Zr atoms and the LiCoO_2 (Figure 5c). The Zr 3d spectrum of the LiCoO_2 film modified under an oxygen pressure of 30 Pa can be analyzed with two components of ZrO_2 (Zr 3d_{5/2}: 183.1 eV) and ZrO_xF_y (Zr 3d_{5/2}: ~184.2 eV).^[32] The Zr 3d peaks shifted to higher B.E. regions than that observed for the pristine surface (ZrO_{2-x} : 182.0 eV), which suggests the ZrO_{2-x} surface layer reacts with PF_6^- , carbonates species and HF in the electrolyte during charge-discharge cycling. For the LiCoO_2 film modified under 1 Pa, the Zr 3d spectrum can be analyzed with two components of ZrO_{2-x} (Zr 3d_{5/2}: 182.1 eV) and ZrO_xF_y (Zr 3d_{5/2}: 183.9 eV). In contrast to that modified under 30 Pa, the ZrO_{2-x} surface layer remains at the interface after charge-discharge cycling. The XPS analysis results for the O 1s and Zr 3d spectra suggest that the reaction process of the CEI formation is strongly related to the interaction between the LiCoO_2 cathode and the ZrO_{2-x} modification layer.

To reveal the surface structure after charge-discharge cycling, the structure of the CEI layer was considered in terms of atomic ratios estimated from XPS results. Figure 6 shows the

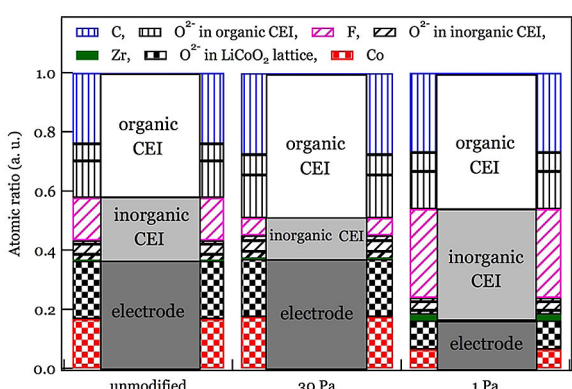


Figure 6. Atomic ratio estimated from XPS spectra classified into the electrode, the inorganic CEI, and the organic CEI.

atomic ratios of components studied in the XP spectra. Components are classified into three major parts: 1) Electrode composed of O (lattice O^{2-} in LiCoO_2) and Co 2p; 2) Inorganic CEI composed of O (O in Zr–O and Co–O, LiOH, ZrO_xF_y and $\text{Li}_x\text{PF}_y\text{O}_z$, Zr 3d, and F 1s; 3) Organic CEI composed of O (alkyl carbonates) and C 1s. The total ratio of CEI components at the unmodified LiCoO_2 surface is 0.6, where organic:inorganic CEI ≈ 2.0:1. The LiCoO_2 surface modified under 30 Pa exhibits a total ratio of CEI layers of 0.6, where organic:inorganic CEI ≈ 3.6:1. In contrast, the LiCoO_2 surface modified under 1 Pa exhibits a total ratio of CEI layers of 0.8, where organic:inorganic CEI ≈ 1.2:1. In addition to increased thickness, a higher ratio of inorganic CEI is observed at the LiCoO_2 surface modified under 1 Pa than for the unmodified LiCoO_2 surface or LiCoO_2 surface

modified under 30 Pa, which means an inorganic-rich CEI grew on the Zr–O–Co surface in the former case. In particular, an increase in the atomic ratio of F was observed. The composition ratios of fluoride compounds were not significantly different between the samples, with around 80% LiF and 20% $\text{Li}_x\text{PF}_y\text{O}_z$ (see supplemental information (S3)). Veider *et al.* reported that a thicker CEI layer containing more numerous LiF was observed at the surface of Al_2O_3 -modified LiCoO_2 after charge-discharge cycling in the voltage range of 2.7–4.6 V.^[33b] A simulation study reported the ionic conductivity of LiF, lithium alkoxide (ROLi), and lithium alkyl carbonates (ROCOLi) as $3.4 \times 10^{-7} \text{ S cm}^{-1}$, $1.5 \times 10^{-7} \text{ S cm}^{-1}$, and $1.1 \times 10^{-7} \text{ S cm}^{-1}$ at 308 K, respectively.^[35] Therefore, a LiF-rich layer can offer lower resistance than an organic-rich layer. The LiCoO_2 surface modified under 30 Pa exhibited a lower atomic ratio of F; this seems to be strongly related to the atomic ratio of Zr. The relative intensity of Zr to Co of the LiCoO_2 surface modified under 30 Pa was 0.01 after the 10th discharging, which is much lower than that modified under 1 Pa of 0.3. The CEI phases such as ZrO_2 and ZrO_xF_y formed at the initial reaction process may be easily peeled away due to the low adhesion of the pristine ZrO_{2-x} modification. In the subsequent cycles, the CEI layer is formed at the exposed LiCoO_2 surfaces, which leads to similar components in the CEI to unmodified LiCoO_2 (Figure 5).

The inorganic-rich CEI layer is generally generated first, at the active material surface, and the organic-rich CEI layer is deposited subsequently.^[36] Therefore, the formation of inorganic compounds on the active materials seems to be an important stage in the growth of adhesive CEI layers and their composition. In our results, the Zr–O–Co chemical bonding state at the pristine electrode surface may stabilize conductive inorganic compounds such as ZrO_xF_y and $\text{Li}_x\text{PF}_y\text{O}_z$, which provide a suitable reaction field for the subsequent formation of organic CEI compounds at the interface. In contrast, Zr–O–Zr surfaces, which have no strong chemical bonding with the LiCoO_2 surface, could not sustain such a stable CEI layer. We can speculate that the chemical bonding state between modification layer and active material forms various CEI layers during charge-discharge cycling, although same modification material is used. The different improvements in cell performances by coating inorganic materials reported in previous works can be attributed to non-controlled formation of chemical bonding state at the electrode surfaces.

2.5. Electrochemical Behavior of Thick ZrO_{2-x} Modified LiCoO_2 Surface

The effect of thickness on the LiCoO_2 surface with Zr–O–Co can be evaluated by setting the modified thickness to 5 nm under 1 Pa. A uniform and dense ZrO_{2-x} modification layer was fabricated under an oxygen pressure of 1 Pa by APD, as described in the supplemental information (S4). The APD technique provided highly dense and uniform ZrO_2 film modification. In contrast, thin films deposited by conventional techniques can include contamination^[37] and form island structures.^[38] The 5-nm-thick film deposited by APD could be a

model system for uniform and high adhesive surface modification. The discharge curves of the modified electrodes with 5-nm-thick films are shown in Figure 7a. The normalized discharge capacity decreased to 0.85 at the 15th cycle and 0.71 at the 35th cycle. The average discharge voltage dropped significantly to 3.82 V, 3.64 V, and 3.49 V at the 1st, 15th, and 35th cycle. The cell performance was not improved by modification; in fact, the average discharge voltage was much lower than that for the unmodified sample. The Zr 3d_{5/2} spectrum was located at 182.5 eV before and 182.0 eV after 10 cycles. The modification layer exhibits Zr–O–Zr bonding, including oxygen deficiencies before and after cycling, whereas ZrO_xF_y is not observed after cycling. The peaks in the O 1s spectra are attributed to Zr–O bonding and CEI components, see supplemental information (S5). Figure 7c shows the atomic ratio of components determined from XP spectra. The components were classified in the same way as those in Figure 6. The total ratio of CEI layers is 0.5, with organic:inorganic CEI ≈ 0.8:1. The atomic ratio of the CEI components is lower than for the 0.4-nm-thick ZrO_{2-x}-modified LiCoO₂ under an oxygen pressure of 1 Pa. Additionally, a smaller ratio of organic CEI is observed. These results indicate a thinner and inorganic-richer CEI layer compared to the cases of 0.4-nm-thick modified surfaces for both pressures. It can be interpreted that the chemical bonding state of the top of cathode materials affected the reactivity toward the electrolyte and altered the formation process of CEI layers.

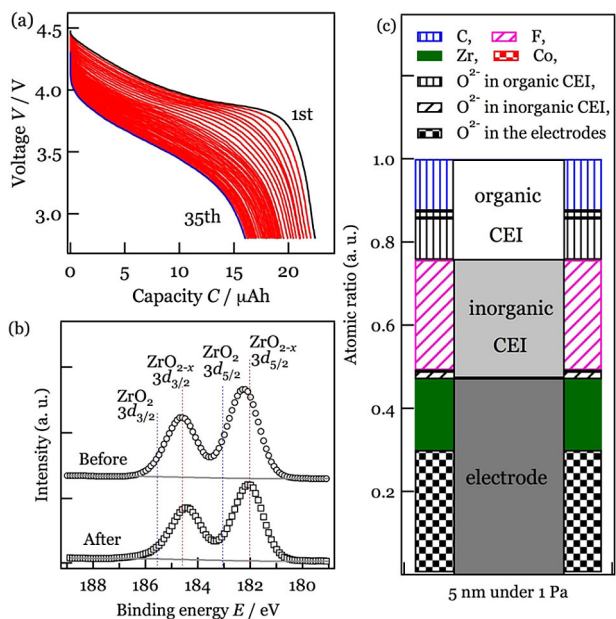


Figure 7. (a) Discharge curves, (b) Zr 3d XP spectra before and after cycling and (c) the atomic ratio estimated from XP spectra classified into the electrode, the inorganic CEI, and the organic CEI of the 5-nm-thick –ZrO_{2-x} modified LiCoO₂.

2.6. Effects of Chemical Bonding States on Stable CEI Formation

Figure 8 presents schematics of the surface structures of LiCoO₂ films modified by (a) 0.4-nm-thick ZrO_{2-x} under an oxygen pressure of 30 Pa, and (b,c) 0.4- and 5-nm-thick ZrO_{2-x} under oxygen pressures of 1 Pa before and after 10 charge-discharge cycles. XPS analyses revealed that surface structures after charge–discharge cycling varied with the initial surface structure. Three types of initial surface structure were determined as follows: 1) A thin ZrO_{2-x}-modified surface without chemical bonding between ZrO_{2-x} and LiCoO₂ (0.4-nm-thick modification under an oxygen pressure of 30 Pa, Figure 8a)

2) A thin ZrO_{2-x}-modified surface with chemical bonding between ZrO_{2-x} and LiCoO₂ such as Zr–O–Co (0.4-nm-thick modification under an oxygen pressure of 1 Pa, Figure 8b)

3) A thick ZrO_{2-x}-modified surface with chemical bonding between ZrO_{2-x} and LiCoO₂ (5-nm-thick film modification under an oxygen pressure of 1 Pa, Figure 8c), with no contact between Zr–O–Co and the electrolyte.

The surface structure of the thin ZrO_{2-x}-modified film without chemical bonding with the LiCoO₂ surface is altered to ZrO₂ or becomes an HF scavenger and forms a ZrO_xF_y layer that is inactive to HF. However, the modification layer can be easily peeled away, simultaneously removing other CEI compounds. Small amounts of Zr were left at the LiCoO₂ surface after the 10th discharging. It is also speculated that the LiCoO₂ surface is not completely covered by a ZrO_xF_y layer. Therefore, side reaction between the exposed LiCoO₂ surfaces and electrolyte could occur continuously in every cycle. Consequently, the CEI layer could acquire a similar structure to that of the unmodified LiCoO₂ surface in later cycles, so cell performances were not much improved. The structure of the thin ZrO_{2-x} modified surface including chemical bonding with the LiCoO₂ surface maintained Zr–O–Co bonding. The atomic ratio attributed to the CEI components increased after the 10th discharge. The ratio of fluoride compounds in the CEI was higher than that for unmodified LiCoO₂. The CEI layer adequately covered the LiCoO₂ surface during the initial 10 charge-discharge cycles. In addition, ZrO_xF_y could remain during charge-discharge owing to Zr–O–Co bonding, strengthening the architecture of the CEI layer. Chemically and physically stable CEI could be formed upon transforming the sustained modification layer during the initial cycling stage, leading to superior cycle retention and a stable average discharge voltage for LiCoO₂. The thick ZrO_{2-x} modification, including chemical bonding with the LiCoO₂ surface, showed Zr–O–Zr bonding at the surface before cycling, which was maintained after cycling. The generated CEI layer was thinner and composed of less CEI organic compounds than in the case of the Zr–O–Co surface. Especially, ZrO_xF_y was not observed. Therefore, the chemical bonding of Zr–O–Co is more effective for stable CEI formation than the Zr–O–Zr bonding in ZrO_{2-x}. The possible mechanisms are as follows. First, the chemical bonding condition in ZrO_{2-x} changes to an unstable and/or high-energy state by forming Zr–O–Co bonding at the ZrO_{2-x}/LiCoO₂ interface, thus the modified ZrO_{2-x} has high reactivity with electrolyte species for the initial CEI formation.

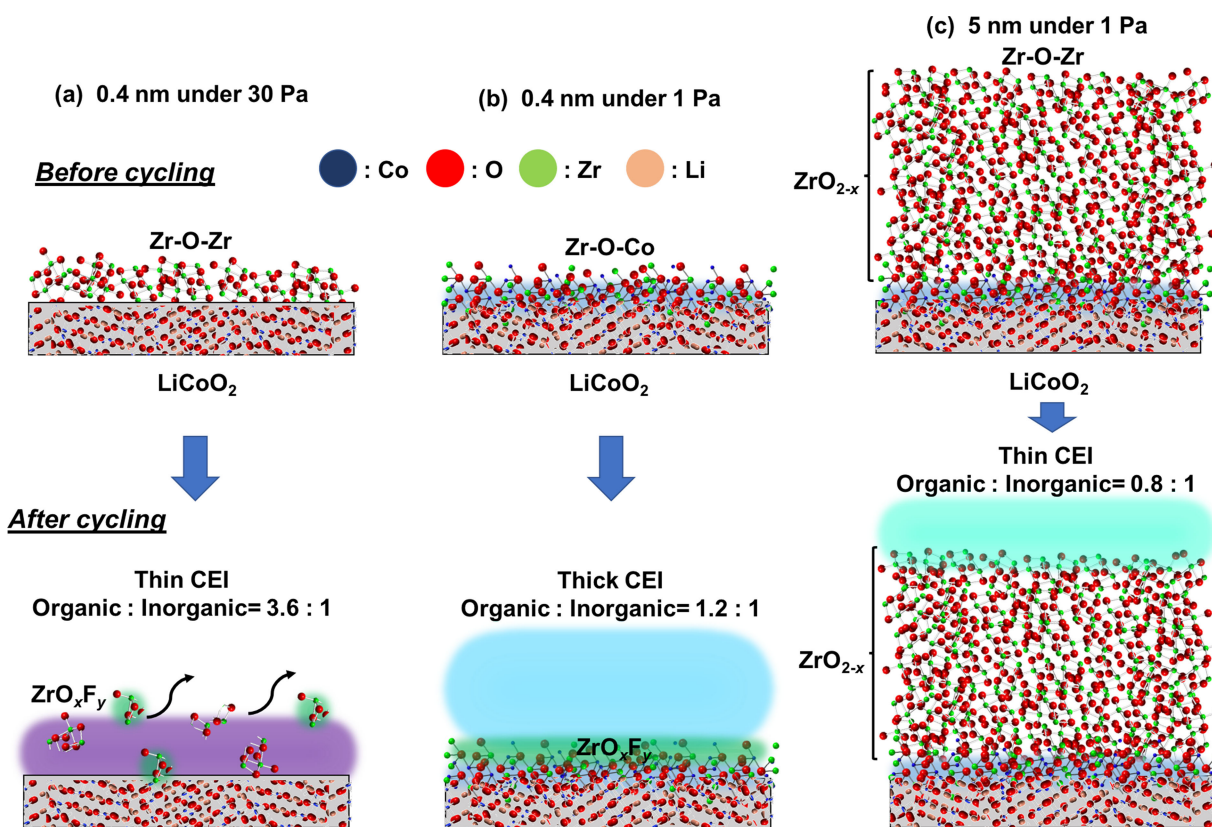


Figure 8. Schematic pictures of the surface structures of LiCoO₂ films modified by (a) 0.4-nm-thick ZrO_{2-x} under oxygen pressures of 30 Pa, and (b) 0.4-nm-thick and (c) 5-nm-thick ZrO_{2-x} under oxygen pressures of 1 Pa before and after 10 cycles of charge-discharge.

As this effect is expected only in a few nanometer regions from the interface, no stable CEI is grown at the 5 nm-thick ZrO_{2-x} modified LiCoO₂ surface, even though Zr–O–Co bonding is formed at the ZrO_{2-x}/LiCoO₂ interface. Second, the chemical bonding between the ZrO_{2-x} modification layer and the LiCoO₂ retains adhesion of the CEI layer grown by reactions with the electrolyte species. Consequently, a layered structure of organic-rich CEI on inorganic-rich CEI is grown on the LiCoO₂ surface, which can provide a stable reaction field for lithium (de) intercalation at high voltage regions.

Representative surface modification techniques such as sol-gel, mechanical milling, and PVD processes require thermal and mechanical energy to be induced to remove contamination and attain uniform mixing.^[6b,9] Consequently, various bonding states could be generated at the cathode surface.^[6b,39] However, the chemical bonding states change depending on synthetic methods and process conditions. In this study, we have successfully controlled the chemical bonding state at the cathode surface and to observe variety of CEI formation by using model LiCoO₂ films and APD. The remaining fluorinated modification layer influenced the functional CEI and helped to improve cell performances. These results are consistent with previous works,^[40] especially that Zr fluoride is stable in the operation voltage.^[41] Controlling the bonding state at the interface revealed that the fluorinated modification layer is not sustained in the case of Zr–O–Zr surfaces owing to low adhesion or reactivity to electrolytes. Zr–O–Zr might not form a

good lithium conduction path between the CEI layer during charge-discharge cycling. Most of all, the chemical bonding states between LiCoO₂ and ZrO_{2-x}, and the reactivity of the modified surface are adjustable parameters for controlling the structures and mechanical and electrochemical properties of the CEI.

3. Conclusions

The effects of chemical bonding at the interface between ZrO_{2-x} and LiCoO₂ on cell performance were demonstrated based on the investigation of surface structure and electrochemical properties. Model LiCoO₂ films surfaces were modified with ZrO_{2-x} coating layers obtained under various oxygen pressures by an APD process to control the ion energy of the evaporated species. XPS analyses of 0.4-nm-thick ZrO_{2-x}-modified LiCoO₂ films indicated that modifications in oxygen pressures from 1 Pa to 30 Pa provided Zr–O–Zr and Zr–O–Co containing surfaces, respectively. The ZrO_{2-x}-modified LiCoO₂ film with Zr–O–Co surfaces exhibited superior cycle retention and stable average discharge voltages in high-voltage operation. In contrast, no clear improvements in cell performance were observed in the case of the 0.4-nm-thick ZrO_{2-x}-modified LiCoO₂ film with the Zr–O–Zr surface. Additionally, the LiCoO₂ film modified by 5-nm-thick ZrO_{2-x} under an oxygen pressure of 1 Pa exhibited a surface containing Zr–O–Zr, which did not

exhibit any improvement of cell performance. *Ex situ* XPS revealed that the Zr–O–Co surface formed highly adhesive inorganic layers such as ZrO_xF_y . Subsequently, thick inorganic-rich CEI was formed. The chemical bonding state between cathode active materials and the modification materials, and reactivity of the electrode surface are controllable parameters that strongly influence the CEI structure and its properties.

Experimental Section

LiCoO_2 films were deposited on a polycrystalline Au substrate using a radio-frequency magnetron sputter system (PSAD-3000, AOV Inc.) with a target of LiCoO_2 bonded onto a copper plate (50 mm in diameter, Toshima Manufacturing). The conditions investigated were as follows: RF power: 125 W; duration: 96 min; pressure: 0.75 Pa; ratio of O_2/Ar : 1/4; temperature: room temperature; and distance between the substrate and target: 30 mm. The LiCoO_2 films were post-annealed at 725 °C under an O_2 flow ($0.2 \text{ dm}^{-3} \text{ min}^{-1}$) to improve their crystallinity. The LiCoO_2 film thicknesses were ca. 500 nm and 570 nm as analyzed by a stylus surface profiler (DektakXT, Bruker Co.). Amorphous ZrO_{2-x} was modified on $\text{Al}_2\text{O}_3(0001)$ single crystal substrates as well as LiCoO_2 films at several oxygen pressures using a pulsed APD apparatus (APS-1, Advance Riko Inc.). $\text{Al}_2\text{O}_3(0001)$ substrates were annealed at 1,000 °C for 10 min. A Zr metal target (Toshima Manufacturing, Co. Ltd.) was used as the cathode of the arc plasma deposition system. The discharge energy applied to the Zr target was controlled by the electric capacity C of 1,080 μF and the applied discharge voltage V of -100 V . Discharge counts were set between 4 to 42 pulses for controlling the film thickness. The distance between the target and the substrate was $8 \times 10^{-2} \text{ m}$. Zr was deposited at oxygen pressures of 30 Pa, 1 Pa, and $3 \times 10^{-4} \text{ Pa}$ to control reactivity with evaporated species. The kinetic energy of Zr atoms arriving at the LiCoO_2 surface at 30 Pa, 1 Pa, and $3 \times 10^{-4} \text{ Pa}$ were estimated as $\sim 0 \text{ eV}$, 6 eV, and 115 eV, respectively. The calculation sequence is provided in the supplemental information. The structures of the LiCoO_2 films synthesized by RF magnetron sputtering were evaluated with XRD (Cu $K\alpha$, SmartLab, Rigaku Corp.), Raman spectroscopy (Raman-11, Nanophoton Corp.), AFM (JSPM-5200, JEOL Ltd.), and FE-SEM (S-5500, Hitachi High-Technologies Corp.). The surface-modified structure and the structure of the CEI at the electrode surface were investigated by XPS (Axis Nova, KRATOS ANALYTICAL and ESCA1700R, Ulvac-phi Inc.). The X-ray source was monochromatic Al $K\alpha_1$ (1,486.6 eV). Peak fitting of the detected spectra was performed using the Casa XPS. The binding energy (B.E.) was calibrated using the C_{sp^2} peak of carbon contamination at 284.8 eV. Charge-discharge measurements were performed with a 2032-type coin cell composed of a Li anode and $1 \text{ mol dm}^{-3} \text{ LiPF}_6$ in a 3:7 (vol.) mixture of ethylene carbonate and diethyl carbonate as the electrolyte. The charge-discharge characteristics were examined in the range of 2.8–4.5 V (vs. Li/Li^+) under current densities from $20.6 \mu\text{A cm}^{-2}$ (0.3 C, where 1 C: 273.8 mA g $^{-1}$) to $34.6 \mu\text{A cm}^{-2}$ (0.5 C). *Ex situ* XPS analysis was conducted for the samples after the 10th cycle to investigate structural changes at the electrode surface. For the *ex-situ* XPS measurements, the coin cells were disassembled in an Ar-filled glove box. The electrodes were washed using dimethyl carbonate and dried in vacuum for 15 min. Airtight sample holders were used to transfer samples between glove boxes and XPS chambers.

Acknowledgements

We would like to thank the Ulvac Riko Corp. for providing arc plasma sources. This work was partially supported by a Grant-in-Aid from the Advanced Low Carbon Technology Research and Development Program (ALCA) of the Japan Science and Technology Agency (JST). We also thank the Baba-Motokura group of the Tokyo Institute of Technology for their kind assistance in XPS measurements, Hara group of the Tokyo Institute of Technology for their cooperation in Raman spectroscopy, and the analysis center of Suzukakedai campus of the Tokyo Institute of Technology for FE-SEM observations.

Conflict of Interest

The authors declare no conflict of interest.

Keywords: cathode • electrolyte • interphase • lithium intercalation cathode • lithium-ion batteries • pulsed arc plasma deposition • surface modification

- [1] J. Cho, Y. J. Kim, B. Park, *Chem. Mater.* **2000**, *12*, 3788–3791.
- [2] K. Yamamoto, Y. Orikasa, D. Takamatsu, Y. Koyama, S. Mori, T. Masese, T. Mori, T. Minato, H. Tanida, T. Uruga, Z. Ogumi, Y. Uchimoto, *Electrochemistry* **2014**, *82*, 891–896.
- [3] Z. Chen, J. R. Dahn, *Electrochim. Solid-State Lett.* **2002**, *5*, A213–A216.
- [4] J. Zhang, R. Gao, L. Sun, H. Zhang, Z. Hu, X. Liu, *Electrochim. Acta* **2016**, *209*, 102–110.
- [5] a) D. Takamatsu, S. Mori, Y. Orikasa, T. Nakatsutsumi, Y. Koyama, H. Tanida, H. Arai, Y. Uchimoto, Z. Ogumi, *J. Electrochem. Soc.* **2013**, *160*, A3054–A3060; b) G. Q. Liu, H. T. Kuo, R. S. Liu, C. H. Shen, D. S. Shy, X. K. Xing, J. M. Chen, *J. Alloys Compd.* **2010**, *496*, 512–516.
- [6] a) J. Cho, J.-G. Lee, B. Kim, B. Park, *Chem. Mater.* **2003**, *15*, 3190–3193; b) Y.-C. Lu, A. N. Mansour, N. Yabuuchi, Y. Shao-Horn, *Chem. Mater.* **2009**, *21*, 4408–4424.
- [7] L. Dahéron, R. Dedryvère, H. Martinez, D. Flahaut, M. Ménétrier, C. Delmas, D. Gonbeau, *Chem. Mater.* **2009**, *21*, 5607–5616.
- [8] A. Yano, M. Shikano, A. Ueda, H. Sakaebi, Z. Ogumi, *J. Electrochem. Soc.* **2017**, *164*, A6116–A6122.
- [9] A. Zhou, Q. Liu, Y. Wang, W. Wang, X. Yao, W. Hu, L. Zhang, X. Yu, J. Z. Li, H. Li, *J. Mater. Chem. A* **2017**, *5*, 24361–24370.
- [10] a) K. Hanada, T. Nishiyama, T. Yoshitake, K. Nagayama, *Diamond Relat. Mater.* **2010**, *19*, 899–903; b) Y. Agawa, S. Endo, M. Matsuura, I. Yoshikazu, *Adv. Energy Res.* **2010**, *123–125*, 1067–1070; c) H. Randhawa, *Thin Solid Films* **1988**, *167*, 175–185.
- [11] a) B. K. Tay, Z. W. Zhao, D. H. C. Chua, *Mater. Sci. Eng. R* **2006**, *52*, 1–48; b) M. M. M. Bilek, D. R. McKenzie, R. N. Tarrant, S. H. M. Lim, D. G. McCulloch, *Surf. Coat. Technol.* **2002**, *156*, 136–142.
- [12] P. J. Martin, A. Bendavid, J. M. Cairney, M. Hoffman, *Surf. Coat. Technol.* **2005**, *200*, 2228–2235.
- [13] T. Yoshitake, Y. Nakagawa, A. Nagano, R. Ohtani, H. Setoyama, E. Kobayashi, K. Sumitani, Y. Agawa, K. Nagayama, *Jpn. J. Appl. Phys.* **2010**, *49*, 015503.
- [14] a) E. Ertürk, H. J. Heuvel, *Thin Solid Films* **1987**, *153*, 135–147; b) P. C. Johnson, H. Randhawa, *Surf. Coat. Technol.* **1987**, *33*, 53–62; c) W. Li, X. Liu, A. Huang, P. K. Chu, *J. Phys. D: Appl. Phys.* **2007**, *40*, 2293–2299.
- [15] M. Ménétrier, I. Saadoune, S. Levasseur, C. Delmas, *J. Mater. Chem.* **1999**, *9*, 1135–1140.
- [16] K. Hara, T.-A. Yano, K. Suzuki, M. Hirayama, T. Hayashi, R. Kanno, M. Hara, *Anal. Sci.* **2017**, *33*, 853–858.
- [17] M. Antaya, K. Cearns, J. S. Preston, J. N. Reimers, J. R. Dahn, *J. Appl. Phys.* **1994**, *76*, 2799.
- [18] a) M. Inaba, Y. Iriyama, Z. Ogumi, Y. Todzuka, A. Tasaka, *J. Raman Spectrosc.* **1997**, *28*, 613–617; b) K. Hara, T.-A. Yano, J. Hata, K. Hikima, K.

- Suzuki, M. Hirayama, R. Kanno, M. Hara, *Appl. Phys. Express* **2017**, *10*, 052503.
- [19] A. Ayame, T. Kitagawa, *Bunseki Kagaku* **1991**, *40*, 673–678.
- [20] M. Murphy, M. S. Walczak, H. Hussain, M. J. Acres, C. A. Muryn, A. G. Thomas, N. Silikas, R. Lindsay, *Surf. Sci.* **2016**, *646*, 146–153.
- [21] C. O. De González, E. A. García, *Surf. Sci.* **1988**, *193*, 305–320.
- [22] J. Wang, S. Yang, X. Liu, S. Ren, F. Guan, M. Chen, *Appl. Surf. Sci.* **2004**, *221*, 272–280.
- [23] G. Cherkashinin, K. Nikolowski, H. Ehrenberg, S. Jacke, L. Dimesso, W. Jaegermann, *Phys. Chem. Chem. Phys.* **2012**, *14*, 12321–12331.
- [24] a) J. C. Dupin, D. Gonbeau, H. Benqlou-Moudden, Ph. Vinatier, S. Levasseur, *Thin Solid Films* **2001**, *384*, 23–32; b) L. Dahéron, R. Dedryvère, H. Martinez, M. Ménétrier, C. Denage, C. Delmas, D. Gonbeau, *Chem. Mater.* **2008**, *20*, 583–590.
- [25] M. Matsui, K. Dokko, K. Kanamura, *J. Power Sources* **2008**, *177*, 184–193.
- [26] a) N. Taguchi, H. Sakaue, T. Akita, K. Tatsumi, Z. Ogumi, *J. Electrochem. Soc.* **2014**, *161*, A1521–A1526; b) W. Luo, J. R. Dahn, *J. Electrochem. Soc.* **2011**, *158*, A110–A114; c) Y. Koyama, H. Arai, I. Tanaka, Y. Uchimoto, Z. Ogumi, *J. Mater. Chem. A* **2014**, *2*, 11235–11245.
- [27] R. Dedryvère, S. Laruelle, S. Grugon, P. Poizot, D. Gonbeau, J. M. Tarascon, *Chem. Mater.* **2004**, *16*, 1056–1061.
- [28] a) T. Ohzuku, A. Ueda, *J. Electrochem. Soc.* **1994**, *141*, 2972–2277; b) J. N. Reimers, J. R. Dahn, *J. Electrochem. Soc.* **1992**, *139*, 2091–2097; c) G. G. Amatucci, J. M. Tarascon, L. C. Klein, *J. Electrochem. Soc.* **1996**, *143*, 1114–1123.
- [29] a) Z. Chen, J. R. Dahn, *Electrochim. Acta* **2004**, *49*, 1079–1090; b) S. Sheng, G. Chen, B. Hu, R. Yang, Y. Xu, *J. Electroanal. Chem.* **2017**, *795*, 59–67.
- [30] a) A. Van der Ven, M. K. Aydinol, G. Ceder, *J. Electrochem. Soc.* **1998**, *145*, 2149–2155; b) J. Kikkawa, S. Terada, A. Gunji, T. Nagai, K. Kurashima, K. Kimoto, *J. Phys. Chem. C* **2015**, *119*, 15823–15830; c) H. Wang, Y. I. Jang, B. Huang, D. R. Sadoway, Y. M. Chiang, *J. Electrochem. Soc.* **1999**, *146*, 473–480.
- [31] a) B. J. Hwang, C. Y. Chen, M. Y. Cheng, R. Santhanam, K. Ragavendran, *J. Power Sources* **2010**, *195*, 4255–4265; b) Y. Zhu, X. Luo, H. Zhi, X. Yang, L. Xing, Y. Liao, M. Xu, W. Li, *ACS Appl. Mater. Interfaces* **2017**, *9*, 12021–12034.
- [32] A. P. Rizzato, C. V. Santilli, S. H. Pulcinelli, Y. Messaddeq, A. F. Craievich, P. Hammer, *J. Non-Cryst. Solids* **2004**, *348*, 38–43.
- [33] a) R. Dedryvère, L. Gireaud, S. Grugon, S. Laruelle, J. M. Tarascon, D. Gonbeau, *J. Phys. Chem. B* **2005**, *109*, 15868–15875; b) S. Verdier, L. El Ouattani, R. Dedryvère, F. Bonhomme, P. Biensan, D. Gonbeau, *J. Electrochem. Soc.* **2007**, *154*, A1088.
- [34] H. Bryngelsson, M. Stjerndahl, T. Gustafsson, K. Edström, *J. Power Sources* **2007**, *174*, 970–975.
- [35] P. Guan, L. Liu, X. Lin, *J. Electrochem. Soc.* **2015**, *162*, A1798–A1808.
- [36] a) N. Schulz, R. Hausbrand, C. Wittich, L. Dimesso, W. Jaegermann, *J. Electrochem. Soc.* **2018**, *165*, A833–A846; b) N. Dupré, M. Cuisinier, Y. Zheng, V. Fernandez, J. Hamon, M. Hirayama, R. Kanno, D. Guyomard, *J. Power Sources* **2018**, *382*, 45–55.
- [37] A. M. Kannan, L. Rabenberg, A. Manthiram, *Electrochem. Solid-State Lett.* **2003**, *6*, A16–A18.
- [38] A. Yano, A. Ueda, M. Shikano, H. Sakaede, Z. Ogumi, *J. Electrochem. Soc.* **2016**, *163*, A75–A82.
- [39] Y. Zhao, J. Li, J. R. Dahn, *Chem. Mater.* **2017**, *29*, 5239–5248.
- [40] a) R. A. Quinlan, Y.-C. Lu, D. Kwabi, Y. Shao-Horn, A. N. Mansour, *J. Electrochem. Soc.* **2016**, *163*, A300–A308; b) J. L. Tebbe, A. M. Holder, C. B. Musgrave, *ACS Appl. Mater. Interfaces* **2015**, *7*, 24265–24278.
- [41] M. Aykol, S. Kirklin, C. Wolverton, *Adv. Energy Mater.* **2014**, *4*, 1400690.

Manuscript received: November 10, 2018

Revised manuscript received: December 21, 2018

Version of record online: January 23, 2019